Published in: Superconductor Science and Technology (2015), vol. 28, 015007
Status: Postprint (author's version)

Magnetic shielding performances of $YBa_2Cu_3O_{7-\delta}$-coated silver tubes obtained by electrophoretic deposition

N Devendra Kumar[1,2], Raphael Closset[1], Laurent Wera[2], Rudi Cloots[1], Philippe Vanderbemden[2] and Benedicte Vertruyen[1]
[1]Department of Chemistry, University of Liège, SUPRATECS, B6, B-4000 Liège, Belgium
[2]Department of Electrical Engineering and Computer Science, University of Liège, SUPRATECS, B28, B-4000 Liège, Belgium

Abstract

We report a complete procedure to achieve multilayer $YBa_2Cu_3O_{7-\delta}$ (YBCO) thick films by electrophoretic deposition on silver tubes using a suspension of YBCO powder in butanol. With the aim to optimize the magnetic shielding performances of the coatings, we have carried out an extensive investigation of the influence of the deposition parameters, the multilayer deposition sequence and the intermediate/final heat treatments on the coating microsfructure. Using the optimized conditions, a 24-layer YBCO coating has been successfully prepared on an 80 mm long Ag tube: the melt growth processed multilayered YBCO thick film thus obtained can shield an applied magnetic field of 1.9 mT at 77 K, the highest value per thickness unit reported so far in the literature for these materials.

Keywords: YBCO thick films, magnetic shielding, electrophoretic deposition

1. Introduction

Magnetic shielding is a promising niche application for superconducting materials, which perform better than the standard magnetic metal screens when shielding low-frequency magnetic fields (<1 kHz) [1-5]. The role of the magnetic shield may be (i) to protect the outside world from a high-magnetic field device [6], or (ii) to protect a device from stray magnetic fields [7]. In this latter case, the device itself can be a superconducting device [8], so that cryogenics does not represent an additional requirement. The magnetic shielding performance can be assessed either by a shielding factor 'SF' (defined as the ratio between the applied induction B_a and the induction B_{in} measured inside the screen) or by the magnitude of B_{lim} (maximum magnetic flux density that can be screened for a given shielding factor).

In a first approximation, the value of B_{lim} of a passive superconducting magnetic shield is proportional to the critical current density of the superconductor and the thickness of the walls [5]. Therefore the highest values of B_{lim} reported so far are for bulk superconducting cylinders having wall thickness of a few millimeters [3, 4, 9, 10]. Such bulk samples, however, are essentially synthesized in simple geometries (e.g. hollow tubes or vessels) [11] and are difficult to be formed in complex shapes, which means that large enclosures should contain slits or joints [12, 13]. Since most magnetic shielding applications require tailor-shaped screens [14], the development and optimization of continuous superconducting coatings deposited on substrates without any shape or size limitation is a formidable challenge. In this context, electrophoretic deposition (EPD) [15, 16] appears as a suitable technique since it allows the deposition of coatings on metallic substrates of various geometries and sizes by applying an electric field to a suspension of charged particles, using the metallic substrate as one of the electrodes.

The preparation of $YBa_2Cu_3O_{7-\delta}$ (YBCO) thick films by EPD was reported by several groups, using either ketone-based [17-20] or alcohol-based [21-24] suspensions.

Although the current densities that can be achieved are much lower than those of coated conductors, the possibility of deposition on complex-shaped substrates is a crucial advantage for magnetic shielding purposes. Our group has been studying YBCO deposition by EPD for several years. At first, we focused on the conventional acetone-based suspensions with iodine as dispersing agent [18, 19, 25]. However, the performances of acetone-based suspensions are very sensitive to the water content in acetone [25] and the low boiling temperature of acetone (55 °C) is thought to worsen the formation of cracks. Looking for alternatives, we recently obtained very promising results with an original butanol-based suspension using branched polyethyleneimine (PEI) as a dispersing agent (see [26] for a detailed report of our investigation leading to the identification of PEI as the preferred dispersing agent).

In the present work, we studied the EPD deposition parameters and the conditions of heat treatment of the coatings prepared with the butanol-based suspension. Since the magnetic shielding performances depend on the

intensity of the supercurrent that can flow through the coating, the microstructural criteria for optimization of the coating are (i) high thickness combined with porosity low enough to ensure adequate percolation in the coating and (ii) good connectivity at the grain boundaries between YBCO grains. Meeting the first criterion depends mainly on the optimization of the first stages of the process, i.e. choosing the EPD parameters and the multilayer deposition scheme to minimize the appearance of large cracks in the coating, as reported and discussed in sections 3.1 and 3.2. The second criterion is mainly affected by the final heat treatment, where the melt growth process is taking place (see section 3.3). In the final sections of the paper, the selected experimental parameters were used to deposit YBCO coatings on silver tubes in order to characterize the magnetic shielding properties.

2. Experimental details

A 10 wt% suspension of YBCO powder in 1-butanol was prepared as described in [26] using branched PEI as a dis-persant. YBCO layers were coated on Ag substrates (99.99%, Goodfellow Cambridge England) by EPD using a PS9009TX Apelex source. Optimization of the deposition and heat treatment parameters was carried out with samples deposited on Ag semi-cylindrical substrates (25 mm height, 16 mm diameter) that were shaped from annealed silver sheets. Samples for magnetic shielding measurements were deposited on annealed tubular Ag substrates (80 mm height, 13 mm diameter). Nickel counter-electrodes were shaped and positioned to ensure a constant 10 mm distance between substrate and counter-electrode. After deposition, the coated substrates were withdrawn from the YBCO suspension at a slow speed of 1 mm s^{-1} to minimize the dip-coating effect. In order to favor uniform drying and thereby minimize the risk of cracking, the coated substrates were kept for 10 min in the butanol-rich atmosphere of the EPD enclosure before being transferred to an oven heated at 70 °C for a 30 min drying in air. Heat treatments were carried out in calibrated tubular furnaces with 100 mm long uniform hot zones (±2 °C). When applicable, Ar or O_2 (99.9% pure) flow rates were adjusted to 100 ml min^{-1}.

X-ray diffractograms were collected with a Bruker D8 diffractometer (parallel beam, CuK_α radiation). Differential scanning calorimetry of the YBCO powder was performed in air and argon with a STA449C Jupiter system (Netzsch). Electron micrographs of the coating surfaces and polished cross-sections were recorded in an environmental scanning electron microscope (XL 30 FEG-ESEM, FEI) coupled to an energy-dispersive x-ray (EDX) analysis system (Bruker Quantax). Average crack widths were estimated by measuring the width of all cracks in 500x375 μm^2 micrographs. Electrical resistivity measurements were carried out in a physical property measurement system (PPMS, Quantum design) using the four probe technique and an excitation current of 1 mA. Magnetic shielding measurements of the YBCO-coated tube were carried out in the PPMS as described in [9, 27]. Basically, a dc magnetic field is applied axially and the magnetic induction inside the tube is measured with a Hall sensor coupled to a nanovoltmeter (HP34420). The applied field was swept slowly at a rate of ~12.5 μTs^{-1} [27]. After each increment of 0.2 mT, the field was held for about 1 s in order to measure the magnetic induction inside the tube.

3. Results and discussion

3.1. Deposition time and deposition voltage

The influence of the deposition time and deposition voltage on the deposited mass was investigated using two series of samples: (i) samples from the first series were prepared with constant 50 V deposition voltage and deposition time between 15 s and 300 s; (ii) samples from the second series were prepared with constant 30 s deposition time and deposition voltage between 30 V and 200 V. As shown in figures 1(a) and (b), the deposited mass increases both with time and with voltage, as usually observed in EPD deposition.

The as-deposited coatings appeared free of cracks to the naked eye. However, electron micrographs collected after heat treatment of the coatings for 1 h at 920 °C in air revealed the presence of cracks, as shown in a few representative micrographs in figure 2. The graph in figure 2(h) plots the crack width versus the deposited mass for the samples from the two series and shows that the average crack width tends to increase with the deposited mass. It is well known that granular ceramic films above some critical thickness develop cracks during the drying stage [28, 29]. As reviewed by Besra and Liu [30] in the case of EPD coatings, even when no cracks are seen immediately after drying, the shrinkage of the coating during sintering is significantly different from that of the substrate, resulting in stresses that are relieved by crack formation. This effect is enhanced when inhomogeneities in the density of the as-deposited coating lead to differential densification during sintering [30]. Strategies to avoid cracking in EPD coatings were discussed for example by Sarkar *et al* [31]. The most efficient approaches, such as freeze/supercritical drying or shrinking substrates, cannot be implemented in the present case. In order to minimize cracking, selection of a liquid with low surface tension is recommended to reduce capillary forces [30, 31]. In this respect, both acetone (used in our previous work) and 1-butanol (used in the present work) have surface tension values of 20-25 mN m^{-1} [32], similar to ethanol and much smaller than water

(72 mN m^{-1}). Additionally, replacing acetone (boiling temperature = 55 °C) by 1-butanol (boiling temperature = 120 °C) ensures a lower vapor pressure and a slower evaporation rate, which is generally found to reduce cracking. Considering the results in figure 2(h), it was decided that 50 V-60 s deposition conditions represent a suitable compromise between deposited mass and crack width.

Figure 1. Effect of (a) deposition time and (b) deposition voltage on the deposited mass.

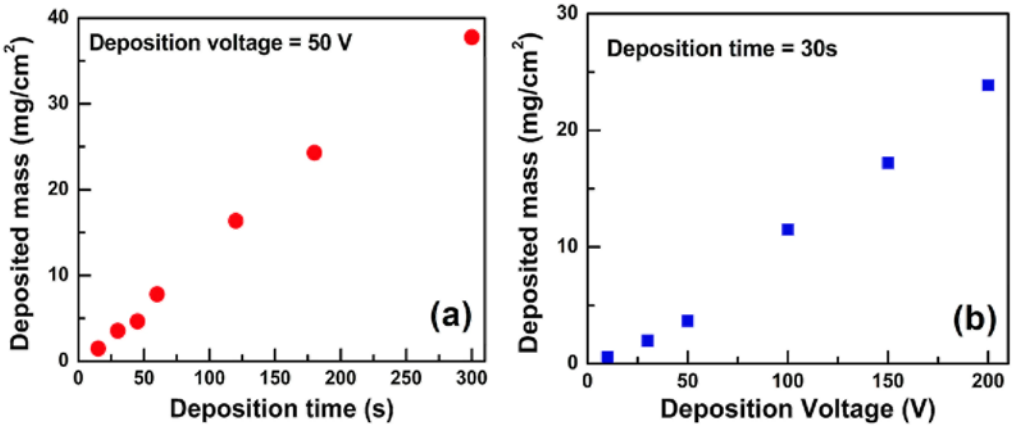

3.2. Multilayer deposition

In the remaining part of the paper, all layers were deposited with 50 V deposition voltage and 60 s deposition time, as selected in the previous section. In order to improve the maximum field that can be shielded (B_{lim}), it is necessary to increase the overall thickness of the coatings by depositing several such layers consecutively. Besides, in order to save time and energy, it would be advantageous to apply the 920 °C heat treatment after deposition and drying of several layers, instead of after each layer. However, this should not come at the cost of an excessive increase in crack width.

Figure 3 compares the surface micrograph of a 3 x 60 s coating (figure 3(a)), prepared using the following sequence: [layer deposition (50 V, 60s)-drying (70 °C, 30 min)]$_3$-920 °C, with the surface micrograph of the 1 x 180 s coating (figure 3(d)) from the first series of samples in section 3.1. Since the deposited mass increases linearly with deposition time (see figure 1(a)) and with the number of (50V, 60s) layers (not shown), the deposited mass is similar in both cases (22 mg cm^{-2} for the 3 x 60 s coating, 24 mg cm^{-2} for the 1 x 180 s coating). However, figure 3 clearly shows that the crack width is much smaller in the case of the 3 x 60 s coating. In addition, the higher magnification micrographs of the 3 x60 s coating (figures 3(b) and (c)) reveal that most cracks affect only one of the layers; in other words, not all cracks propagate through the whole thickness of the coating. A further increase in the number of layers deposited before heat treatment to 920 °C was found to have an adverse effect on the crack width, as shown in figure 3(e) for up to seven consecutive (50 V, 60 s) layers.

Based on the above results, it was decided that the heat treatment at 920 °C in air would be applied after every 3 layers. Figure 4 shows a cross section through a 12-layer coating prepared by depositing four series of three layers according to the sequence {[layer deposition (50 V, 60 s)-drying (70 °C)]$_3$-920 °C}$_4$, followed by an extended heat treatment at a maximum temperature of 920 °C. It is of interest to note that the four sets of layers can still be distinguished because pores are usually not aligned from one set of layers to the next.

Before going on to the optimization of the final heat treatment (see next section), it is worth discussing how the 920 °C temperature was selected for the intermediate sintering in all the experiments presented in this paper. This is important because inappropriate conditions of intermediate sintering may lead to severe cracking of the coating or, in the worst cases, to peeling-off of the coating. The selection criteria rely on concepts of sintering in ceramics [33], which are outlined below and followed by a summary of the experimental results that led to the selection of the intermediate sintering conditions.

The small size of the YBCO particles (below 1 µm) means that there is a significant driving force for the reduction of the surface energy by thermally activated coarsening and densification solid state mechanisms during a heat treatment. The driving force decreases with the progress of coarsening and/or densification, so that the potential for further densification depends on thermal history. In the present case, this means that the choice of the heating rate and temperature for the intermediate sintering affects the microstructure of the coating and its

behavior during the final heat treatment.

Figure 2. (a)-(c) Electron micrographs of the surface of coatings heated for 1 h at 920 °C after EPD deposition at 50 V with different deposition times, (d)-(f) Electron micrographs of the surface of coatings heated for 1 h at 920 °C after EPD deposition during 30 s with different deposition voltages, (g) Photograph of the 50 V, 60 s coating on semi-cylindrical silver substrate heated for 1 h at 920 °C. (h) Dependence of average crack width as a function of deposited mass. Red circle and blue square symbols correspond to samples deposited with various deposition times and deposition voltages, respectively.

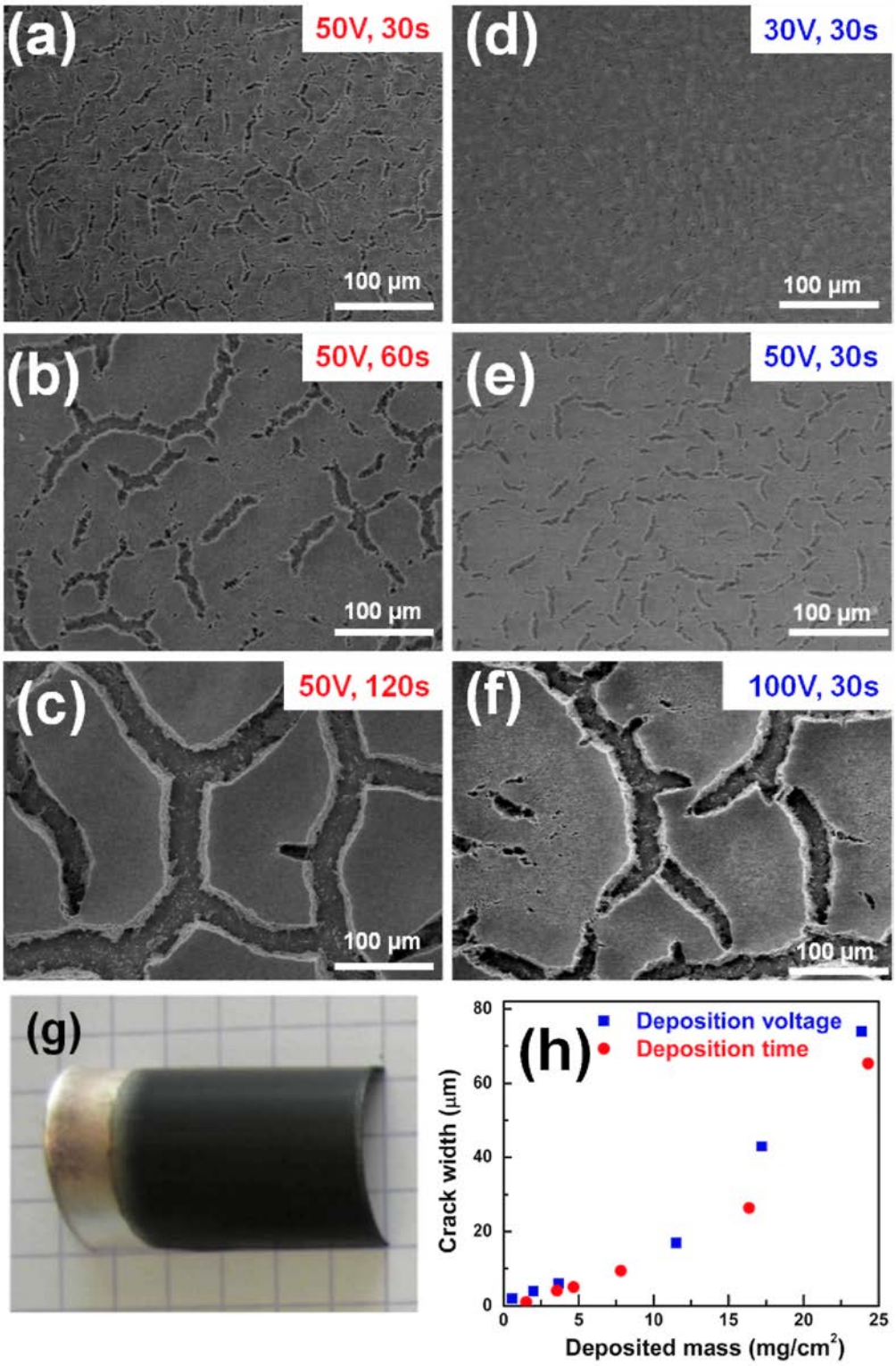

Figure 3. (a), and (b) Melting of silver substrate of coating processed with T_{MAX} of Surface and (c) polished cross-section electron micrographs of a coating heated for 1 h at 920 °C after deposition of three (50 V, 60 s) layers, (d) Surface electron micrograph of a coating heated for 1 h at 920 °C after deposition of one (50 V, 180 s) layer, (e) Influence of the number of (50 V, 60 s) layers on average crack width.

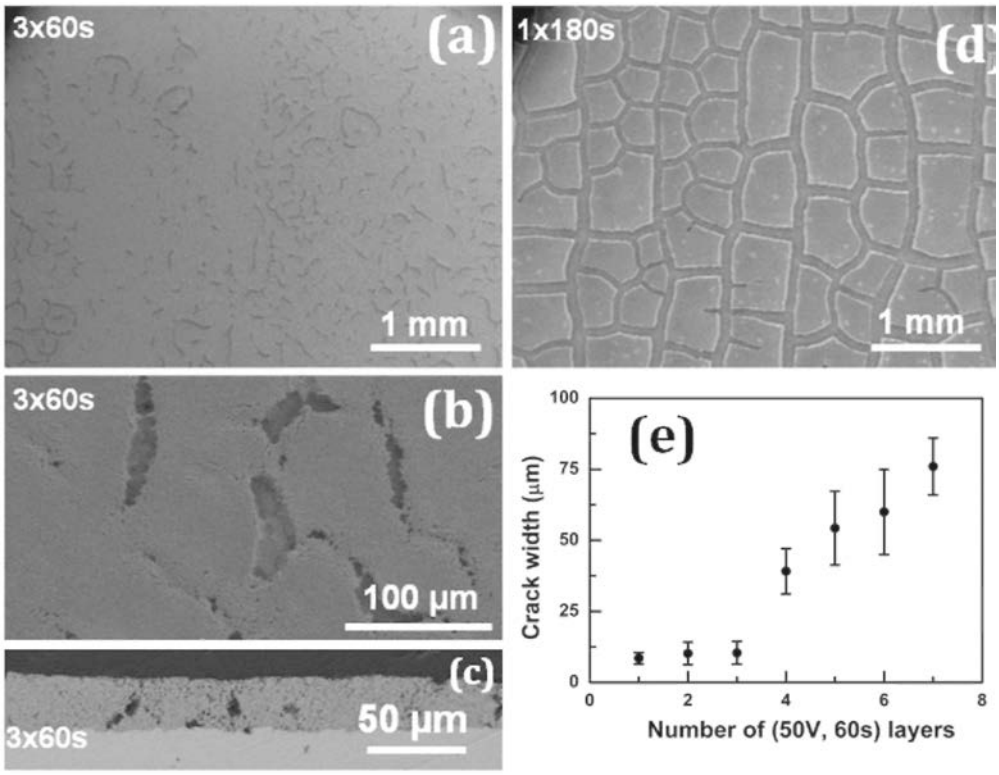

On the one hand, the intermediate sintering temperature should not be too high because rapid densification combined to the existence of drying cracks would result in a coating microstructure with dense islands separated by large macrocracks (as wide as 0.5 mm) that could not be mended by the melt-growth process during the final heat treatment.

On the other hand, the intermediate sintering temperature should not be too low because (i) the formation of necks between the particles is required so that the cohesion of the coating is sufficient to withstand handling and deposition of further layers and (ii) the residual driving force for densification must be low to prevent cracking by rapid densification when the temperature is further increased during the final heat treatment.

The influence of the heating rate results from the fact that coarsening is favoured at lower temperatures while densification becomes fast at higher temperatures. Therefore using a fast heating rate means that not much driving force is spent during the heating period and rapid densification is to be expected at the dwell temperature. Another point to consider regarding the heating (and cooling) rate concerns the difference in thermal expansion [34, 35] between the coating and the silver substrate. It is likely to have more severe consequences if the sample is heated/cooled very fast or is placed directly at high/low temperatures, because the difference in thermal diffusivity [36, 37] means that the silver substrate could reach the final temperature before the coating so that mechanical stress on the coating is larger and the propagation of cracks may result in peeling off.

Experimentally, we optimized the intermediate sintering conditions by testing the adhesion of coatings through immersion of the coated substrates in ethanol and application of ultrasonication for 2min. We found that the coatings submitted to intermediate sintering at temperatures lower than 920°C suffered from partial peeling off from the substrate during ultrasonication. Coatings heated at 920°C during intermediate sintering did not crack or peel away during final heat treatments at higher temperatures, indicating that the residual driving force for solid state densification mechanisms was low enough. 920°C was therefore selected as the optimum temperature for intermediate sintering. Further adhesion tests showed that in the case of intermediate sintering at 920 °C, the heating/cooling rate could be increased to $300°Ch^{-1}$ (instead of $100°Ch^{-1}$) without loss of adhesion. However, even faster heating and cooling rates achieved by placing and removing the samples from a pre-heated furnace resulted in partial peeling off from the substrate. Therefore the $300°Ch^{-1}$ rate was adopted in subsequent experiments, since it allows for a substantially faster heat treatment.

3.3. Final heat treatment

A multilayer coating such as shown in figure 4 requires an additional heat treatment to achieve adequate superconducting properties. Indeed, the maximum temperature of 920 °C in air that is applied to the coating during the multilayer deposition is not high enough to ensure high quality contacts between YBCO grains. The results reported in the present section concern the optimization of a final heat treatment for 12-layer coatings prepared according to the sequence {[layer deposition (50 V, 60s)-drying (70 °C)]$_3$-920 °C}$_4$.

Since the coatings are deposited on silver substrates, the temperature of the final heat treatment must be chosen so that the Ag substrate (melting temperature = 961 °C in air) does not melt or become too soft but, at the same time, does reach a temperature high enough for incongruent melting of the YBCO phase. The peritectic temperature (T_p) of the YBCO powder used in this work was measured by thermal analysis (not shown) and found to decrease from ~1005 °C in air to ~935 °C in argon, in agreement with literature [38] but without taking into account that the silver substrate might cause a further decrease of T_p [39].

Figure 4. Electron micrographs of the polished cross-section of a 12-layer coating. The micrograph in (b) is the magnified image of the region marked in (a). The 4 sets of three layers can be distinguished even after the 920 °C heat treatment as marked by double-ended arrows next to micrograph (b).

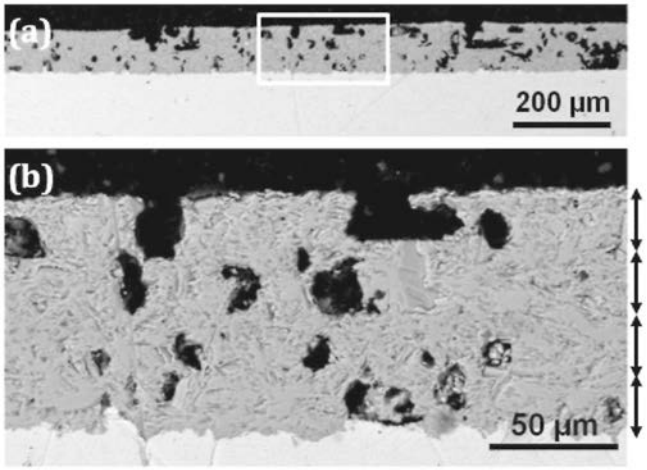

Preliminary tests were performed for the melt growth step of the final heat treatment in argon atmosphere at maximum temperatures T_{MAX} ranging from 920 °C to 960 °C. The electron micrograph of the coating treated to 920 °C (figure 5(a)) shows a microstructure typical of solid state sintering, where many 1-2 µm diameter (sub) grains are still easily distinguished. At the other end of the T_{MAX} range, heating up to 960 °C caused the melting of the silver substrate, as shown in figure 5(b).

Considering these results, 920 °C and 960 °C were rejected and a detailed study was carried out for three values of T_{MAX} of 930 °C, 940 °C and 950 °C in argon atmosphere with the temperature profile shown in figure 5(c). Electron micrographs of these coatings are shown in figures 5(d)-(g). In figure 5(d), the coating heated to 930 °C displays larger and more anisotropic grains compared to the 1-2 µm particles observed during the preliminary test at 920 °C: these 5-10 µm long platelet-shaped grains coexist with larger blocks where fusing of neighboring grains has occurred. Increasing T_{MAX} to 940 °C leads to a microstructure (figure 5(e)) mainly constituted of such well-fused blocks, with a few individual grains decorating the extreme surface of the coating. Further increasing T_{MAX} to 950 °C leads to some deformation of the silver substrate (not shown) and to surface and cross-section microstructures (figures 5(f) and (g)) where large zones of Ba-rich solidified liquid phase (highlighted in yellow) were identified by EDX.

The results at 930 °C, 940 °C and 950 °C are consistent with the following picture. Increasing T_{MAX} from 930 °C to 940 °C leads to an increase in the formation of liquid phase by peritectic decomposition, followed by the formation of blocks of well-fused grains with good inter-grain connections during the slow cooling process (through peritectic recombination of solid Y_2BaCuO_5 and the liquid phase). In the case where T_{MAX} is 950 °C, the incongruent melting of the YBCO phase is more severe, causing larger liquid phase content in the sample. Additionally, due to the higher temperature, the viscosity of the liquid phase decreases. This results in a partial segregation of the liquid phase in the large pores, with percolation to the surface of the samples leading to oozing out problems. Hence these samples exhibit inhomogeneous microstructures with large liquid phase reservoirs

and randomly distributed yttrium rich Y_2BaCuO_5 regions, which affects the peritectic recombination to a considerable extent. It should be noted that the microstructures and scenario described here are different from the melt-growth processing of bulk samples, where (i) yttrium-rich flux is provided by addition of an excess of Y_2BaCuO_5 to precursor powders to aid the growth of $YBa_2Cu_3O_{7-\delta}$, (ii) seed crystals with higher peritectic temperatures T_p are employed to orient the growth of YBCO and (iii) PtO_2/CeO_2 which can be used as grain refiners influence the liquid phases to some extent during melt processing [40, 41].

Figure 5. (a) Surface electron micrographs of coatings processed with T_{MAX} of 920 °C. (b) Melting of silver substrate of coating processed with T_{MAX} of 960 °C. (c) Temperature profile of the final heat treatment followed to test maximum temperatures T_{MAX}: 930 °C-940 °C-950 °C. (d)-(g) Electron micrographs of coatings processed with T_{MAX} of 930 °C, 940 °C or 950 °C respectively. The large grains and cracked zones highlighted in yellow in (d) and (e) correspond to solidified liquid phase as ascertained by EDX analysis (not shown).

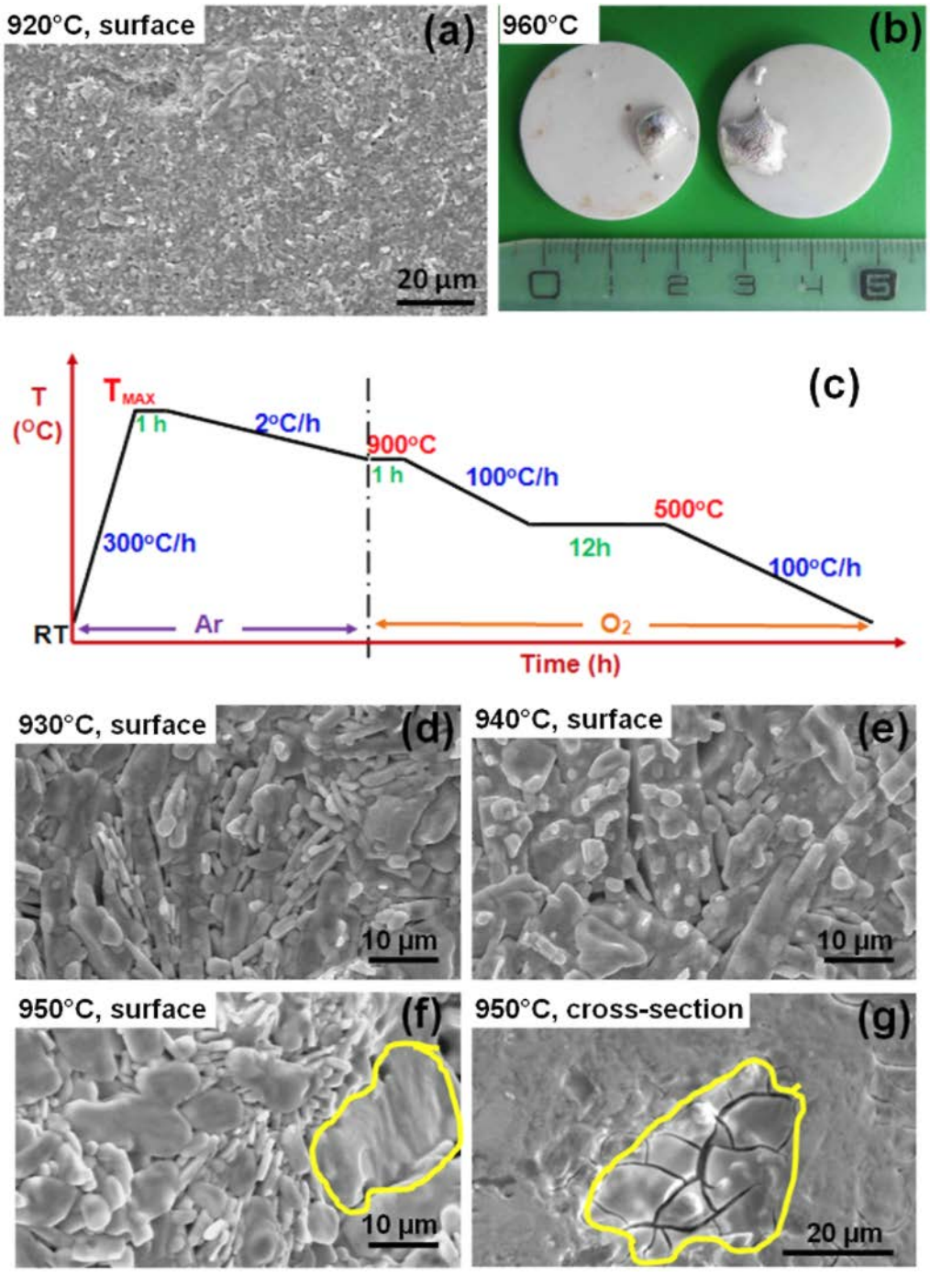

In view of the above results, a maximum temperature of 940 °C appears to be the optimum choice for the final heat treatment of EPD-processed multilayers, as confirmed by a sharp superconducting transition at 92 K [26].

It is well known that YBCO must be in its oxygen-rich, orthorhombic phase to display superconducting properties. Therefore care must be taken to adjust the oxygen content in the coatings. In all cases, a slow cooling rate was used from T_{MAX} to 900 °C to allow for the recombination of Y_2BaCuO_5 and the liquid phase into $YBa_2Cu_3O_{7-\delta}$. The shift from argon atmosphere to oxygen atmosphere was never performed at temperatures higher than 900 °C to make sure that no quenching of liquid phase could occur due to an abrupt increase of T_p induced by the oxygen atmosphere. The influence of a decrease in the cooling rate after oxygen entry was investigated by comparing samples prepared with 100 °Ch^{-1} or 20 °Ch^{-1} cooling rates from 900 °C to 850 °C but no significant differences were observed in the electron micrographs and EDX maps of the two samples (not shown). Since a slower cooling rate is expected to be beneficial in terms of peritectic recombination reactions, the 20 °Ch^{-1} cooling rate was adopted for the preparation of the multilayer coating on silver tube (see section 3.4). Even when oxygen is introduced at 900 °C, an oxygenation step still needs to be performed in the ~450-500 °C temperature range to increase the oxygen content of the YBCO phase. This is standard practice for bulk superconductors [42-44]. In the case of porous films with typical thickness in the 100-200 µm range, it was interesting to check whether the 12 h plateau at 500 °C could be decreased to 6h in order to reduce the overall duration of the final heat treatment. These two samples were compared in a magnetic repulsion test conducted in liquid nitrogen employing a small permanent magnet: the sample which was oxygenated for 6h did not show any repulsion, unlike the other sample. Hence the oxygenation time at 500 °C was kept at 12 h.

Figure 6. (a) Temperature profile of the final heat treatment applied to the YBCO-coated tube, (b) Photograph of the YBCO-coated tube after final heat treatment, (c) X-ray diffractogram of the YBCO-coated tube surface after final heat treatment with indexation of the reflections of the orthorhombic $YBa_2Cu_3O_{7-\delta}$ phase and identification of the reflections of Y_2BaCuO_5 (Y-211) and silver, (d) Electron micrograph of the tube surface.

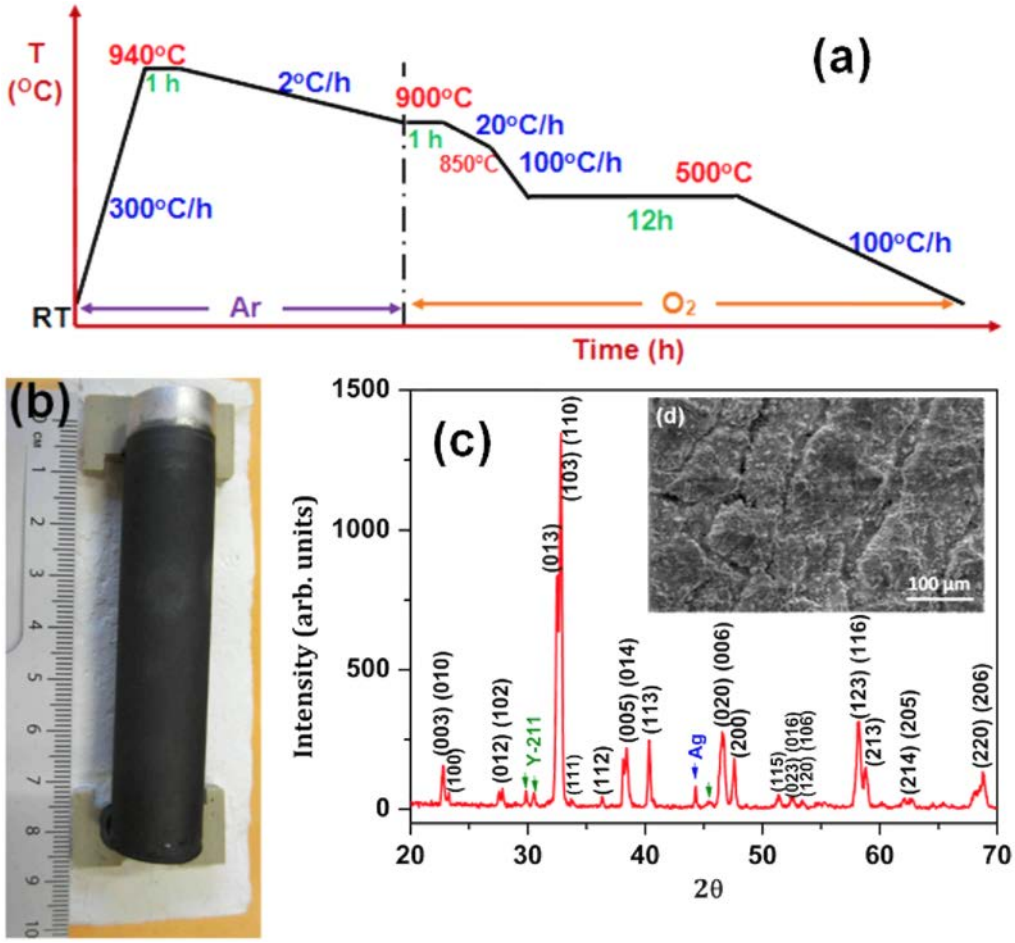

Figure 7. (a), (b) Electron micrographs of a polished cross-section through the YBCO-coated tube, (c)-(f) EDX maps of the area framed in (b).

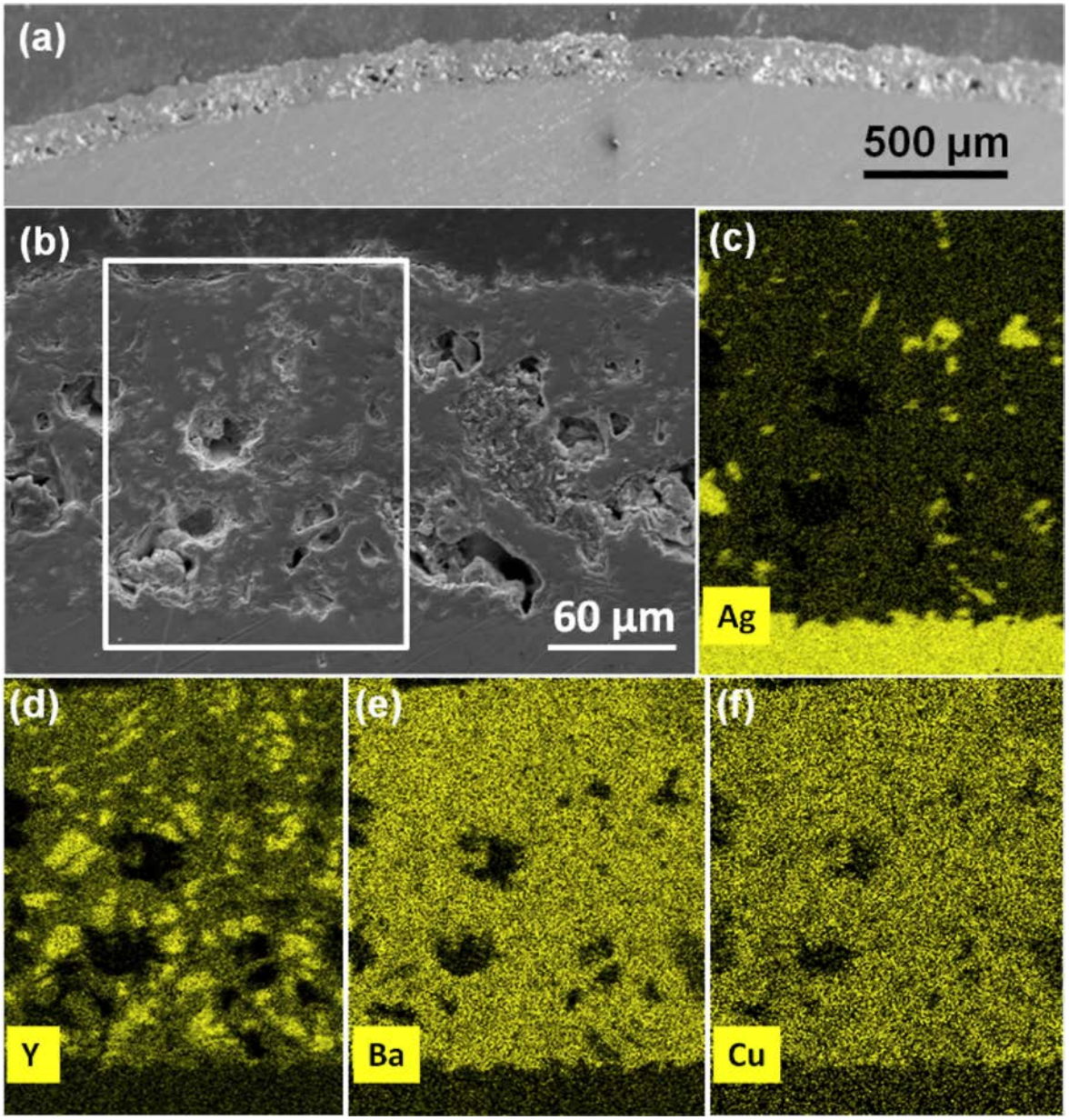

3.4. Multilayered YBCO thick films on Ag tube

The experimental conditions selected during the optimization procedure reported in the previous sections were used to prepare a multilayer YBCO coating on an Ag cylinder in order to study its magnetic shielding properties. A 244ayer coating was deposited according to the sequence {[layer deposition (50 V, 60s)-drying (70ºC)]$_3$-920°C}$_8$ and submitted to the final heat treatment depicted in figure 6(a). A photograph of the processed YBCO-coated tube is shown in figure 6(b).

The XRD pattern collected on the surface of the tube (figure 6(c)) could be indexed with orthorhombic YBCO as the major phase, small amounts of Y_2BaCuO_5 and silver. An electron micrograph of the tube surface (figure 6(d)) shows that cracks in the upper layers do not extend through the whole thickness of the coating. After completion of the magnetic shielding measurements (see later, section 3.5), the tube was cut, set into resin and polished to obtain information about the microstructure and phase distribution. Electron micrographs of the polished cross-section are shown in figures 7(a) and (b). The thickness of YBCO layer is ~150 µm. The low magnification micrograph in figure 7(a) reflects the homogeneity in the thickness of the film. As expected for melt growth processed samples, the coating possesses significant porosity with pore size in the range 10-70 µm.

The composition homogeneity of the coating was investigated by EDX mapping of yttrium, barium, copper and silver signals. As a typical example, figures 7(c)-(f) show EDX maps of a 145x180 μm^2 area framed in the micrograph of figure 7(b). Some diffusion of Ag in the YBCO coating is observed. The yttrium-rich regions in the matrix were identified as Y_2BaCuO_5 embedded in YBCO from the atomic ratios of Y, Ba and Cu in EDX spectra.

Figure 8. (a) Magnetic induction inside the tube (B_{in}) when the applied field ($\mu_0 H_a$) is cycled from 0 up to 80 mT and back to 0 at several temperatures between 20 K and 77 K. (b) Same data as the field increasing branch, plotted as shielding factor ($\mu_0 H_a/B_{in}$) versus applied field ($\mu_0 H_a$). It can be seen that the sample is able to shield applied magnetic fields of ~ 1.9 mT at 77 K and ~8.2 mT at 20 K.

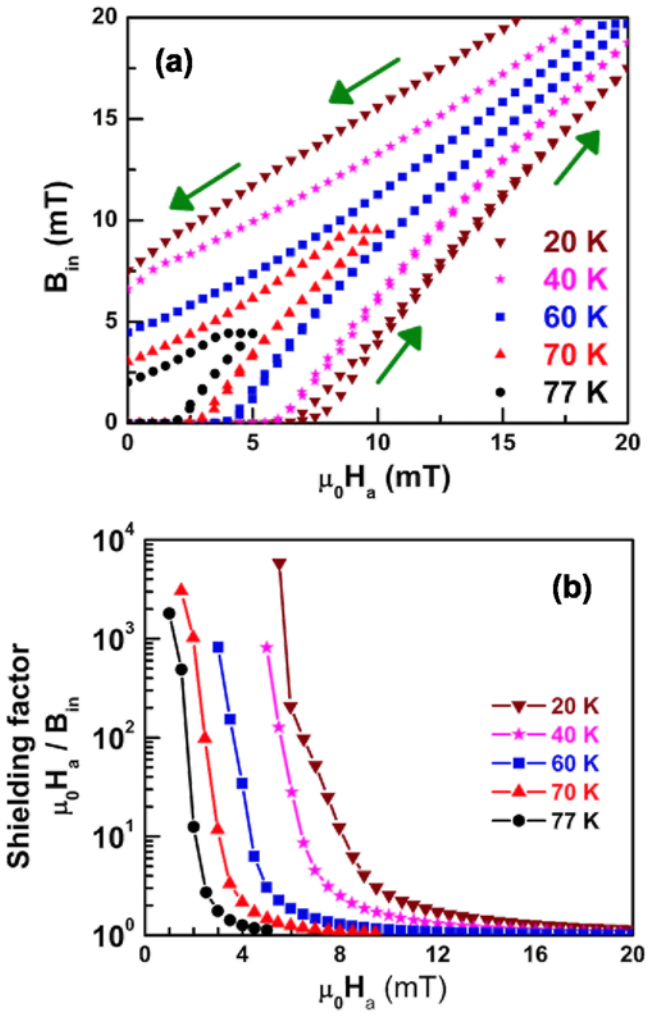

3.5. Magnetic Shielding Properties

The magnetic shielding properties of the YBCO-coated tube described in the previous section were measured at different temperatures between 20 and 77 K by applying magnetic field $\mu_0 H_a$ up to 80 mT. The results are shown in figure 8. Figure 8(a) shows the induction inside the tube (B_{in}) versus applied field ($\mu_0 H_a$) when the applied field is cycled from 0 up to 80 mT (increasing fields) and back to 0 (decreasing fields). Figure 8(b) shows a plot of shielding factor ($\mu_0 H_a/B_{in}$) corresponding to the increasing field branch shown in figure 8(a).

The YBCO-coated tube shows a threshold induced field 'B_{lim}' (defined as the field above which the shielding factor becomes smaller than 10) of ~1.9mT at 77 K. This value increases to ~8.2 mT when the temperature is 20 K. The value for B_{lim} is determined from each of the curves in figure 8(b) and its temperature dependence is shown in figure 9(a). From B_{lim} and the thickness of the YBCO superconducting layer (~150μm), the critical current density J_c can be estimated from the Bean model [45]. If, as a first approximation, the critical current density is assumed to be field-independent, one obtains an average $J_c \sim 10^3$ A cm^{-2} at 77 K. In a second approximation, J_c can be assumed to be field-dependent and follow a Bean-Kim law [46] and the full J_c(B) curve

can be computed from the hysteresis cycle (figure 8(a)) following the procedure reported in [47]. The field dependence of the J_c at 77 K is shown in figure 9(b). The zero field value of J_c resulted as 3600 A cm^{-2} .

Figure 9. (a) Temperature dependence of shielding field (B_{lim}) of the YBCO-coated tube. (b) Field dependence of J_c obtained for the YBCO-coated tube at 77 K.

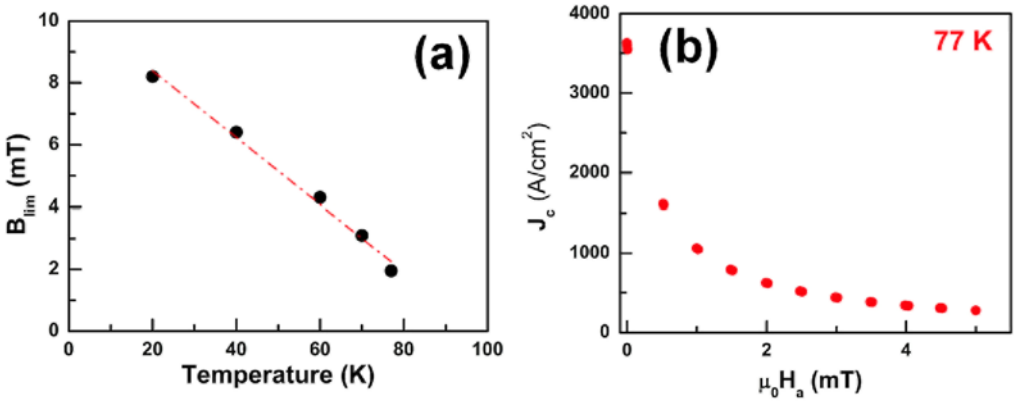

Table 1. Comparison of shielding properties at 77 K (both in bulk and thick film configurations)

	Shaping method	Shielding field (B_{lim})	Thickness	Dimensions of the bulk/substrate (cm)			Reference
				L	OD	ID	
Bulks							
Disk[a]	Pressed	3 mT	40 mm	4	NR	NR	[48]
Tube	Hydrostatic pressing	0.7 mT	2 mm	10	2	1.6	[49]
Tube	Pressed	1.6 mT	1.9 mm	2.3	0.88	0.5	[50]
Tube	Axial compression	1.2 mT	10 mm	5	NR	NR	[51]
Tube	Isostatic compression	1.2 mT	10 mm	5	NR	NR	[51]
Tube	Isostatic compression	2.3 mT	1.2 mm	4	NR	NR	[48]
Tube	Pressed	2.8 mT	0.33 mm	5	1.56	0.9	[52]
Tube[b]	Pressed	1.8 mT	1.9 mm	2.3	0.88	0.5	[50]
Tube[c]	Isostatic compression	1.6 mT	8 mm	5	NR	NR	[51]
Coatings							
On stainless steel plate	Plasma spray	0.7 mT	180 μm		Planar substrate: 45x45x1.5 mm^3		[53]
On Ag tube	Continuation detonation spray	0.1 mT	40 μm	20	2	1.9	[54]
On Ag tube	Continuation detonation spray	0.15 mT	75 μm	20	2	1.9	[54]
On Ag tube	Electrophoretic deposition	0.015 mT	50 μm	20	2	1.9	[54]
On Ag tube	Electrophoretic deposition	0.25 mT	40 μm	10	NR	2	[55]
On Ag tube	Electrophoretic deposition	1.3 mT	100 μm	8	1.6	1.3	Our previous work [26]
On Ag tube	Electrophoretic deposition	1.9 mT	150 μm	8	1.6	1.3	Present work

Note: L—length, OD—Outer diameter, ID—Inner diameter, NR—Not reported.
[a] YBCO+Ag.
[b] YBCO+7 wt% Ag.
[c] YBCO+10 wt% Ag.

These results show that the large pores and the significant amount of Y_2BaCuO_5 (described in section 3.4) do not seriously impede current flow in the coating. In theory, a decrease in porosity and/or in Y_2BaCuO_5 content should enhance the shielding properties by increasing the effective cross section for current flow. However, porosity facilitates oxygenation and a decrease in the cooling rate in the hope to improve peritectic recombination would significantly extend the processing time. In any case, it should be stressed that the B_{lim} value of ~ 1.9 mT at 77 K obtained here is the best reported so far in the literature for an YBCO coating and only a few of the much thicker bulk screens display higher values (see table 1). It is also of interest to compare the results obtained in this work (24 layers, thickness 150 µm, B_{lim} ~ 1-9 mT) to those obtained in our earlier work [26], i.e. 12 layers, thickness 100 µm, B_{lim} ~ 1.3 mT. Remarkably, the B_{lim} correlates almost perfectly with the thickness of the superconductor (1.9 ~ 1.3 x 1.5), giving evidence that the critical current density J_c is not degraded in the thicker sample. The fact that the coating thickness, however, is not proportional to the number of layers shows that e.g. doubling further the number of layers would not lead to doubling B_{lim}. If much higher B_{lim} values are required, we would rather recommend to combine several concentric shields (having each a B_{lim} of approx. 2-3 mT) in order to obtain an overall B_{lim} in excess of 10 mT (at 77 K) if such a value is necessary for a targeted application.

4. Summary and conclusions

We have shown that it is possible to achieve thickness above 100 µm for multilayer YBCO coatings prepared by EPD on silver, thanks to a systematic optimization of the experimental parameters at the different stages of the process: deposition of individual layers, intermediate sintering, multilayer deposition sequence and final heat treatment. Preparation of such thick coatings is notoriously difficult because of their tendency to form macrocracks or, in the worst cases, to peel off from the substrate. Addressing this issue involves two key points, discussed in detail in the paper. First, the formation of drying cracks must be controlled by depositing individual layers that are below a critical thickness. Second, the temperature and heating rate of the intermediate sintering must be selected to achieve an intermediate level of densification, in order to ensure adhesion of the coating and a low residual driving force for further densification in the solid state. In the last stage of the optimization, the parameters of the final heat treatment have been selected to achieve adequate superconducting properties through melt-growth processing.

When prepared with the optimized deposition conditions and heat treatments, a 150 µm thick YBCO coating obtained by depositing 24 layers on an 80 mm long Ag cylindrical tube shows shielding properties better than 1.9 mT at 77 K, a highest reported value per thickness unit so far for these materials in the literature. The shielding properties of the present sample are compared to the best ones reported in literature. The present methodology is efficient in delivering high quality thick films and hence is technologically significant for magnetic shielding applications.

Acknowledgements

Authors thank the Office of Naval Research, USA for the financial support provided. This work relates to Department of the Navy Grant N62909-10-1-7152 issued by Office of Naval Research Global. NDK gratefully acknowledges the financial support (opportunity grant) received from University of Liege, Belgium. The authors thank the Center for Applied Microscopy (CATµ) for the microscopy support.

References

[1] Pavese F 1998 *Handbook of Applied Superconductivity* (Bristol: Institute of Physics) p 1461

[2] Caputo J G, Gozzelino L, Laviano F, Ghigo G, Gerbaldo R, Noudem J, Thimont Y and Bernstein P 2013 *J. Appl. Phys.* 114 233913

[3] Gozzelino L *et al* 2011 *J. Supercond. Novel Magn.* 24 307

[4] Rabbers J J, Oomen M P, Bassani E, Ripamonti G and Giunchi G 2010 *Supercond. Sci. Technol.* 23 125003

[5] Denis S, Dusoulier L, Dirickx M, Vanderbemden P, Cloots R, Ausloos M and Vanderheyden B 2007 *Supercond. Sci. Technol.* 20 192

[6] Hofman M B, Kuijer J P, de Ridder J W, Perk L R and Verdaasdonk R M 2013 *Med. Phys.* 40 012303

[7] Gömöry F, Solovyov M, Souc J, Navau C, Prat-Camps J and Sanchez A 2012 *Science* 23 1466

[8] Sternickel K and Braginski A I 2006 *Supercond. Sci. Technol.* 19 S160

[9] Fagnard J-F, Elschner S, Bock J, Dirickx M, Vanderheyden B and Vanderbemden P 2010 *Supercond. Sci.*

Technol. 23 095012

[10] Gozzelino L, Agostino A, Gerbaldo R, Ghigo G and Laviano F 2012 *Supercond. Sci. Technol.* 25 115013

[11] Plechacek V, Hejtmanek J, Sedmidubsky D, Knizek K, Pollert E, Janu Z and Tichy R 1995 *IEEE Trans. Appl. Supercond.* 5 528

[12] Denis S, Dirickx M, Vanderbemden P, Ausloos M and Vanderheyden B 2007 *Supercond. Sci. Technol.* 20 418

[13] Fagnard J-F, Elschner S, Hobl A, Bock J, Vanderheyden B and Vanderbemden P 2012 *Supercond. Sci. Technol.* 25 104006

[14] Masson P, Netter D, Leveque J and Rezzoug A 2001 *IEEE Trans. Appl. Supercond.* 11 2248

[15] Van der Biest O O and Vandeperre L J 1999 *Annu. Rev. Mater. Sci.* 29 327

[16] Boccaccini A R and Zhitomirsky I 2002 *Curr. Opin. Solid State Mater. Sci.* 6 251

[17] Soh D, Shan Y-Q, Park J, Li Y and Cho Y 2000 *Physica* C 337 44

[18] Dusoulier L *et al* 2006 *Key Eng. Mater.* 314 153

[19] Dusoulier L, Denis S, Vanderbemden P, Dirickx M, Ausloos M, Cloots R and Vertruyen B 2006 *J. Mater. Sci.* 41 8109

[20] Nojima H, Shintaku H, Nagata M and Koba M 1991 *Japan. J. Appl. Phys.* 30 LI 166

[21] Sarkar P, Mathur S, Nicholson P S and Stager C V 1991 *J. Appl. Phys.* 69 1775

[22] Casan-Pastor N, Gómez-Romero P, Fuertes A and Brossa M 1993 *Solid State Ionics* 66 241

[23] Das Sharma A, Sen A and Maiti H S 1993 *Ceram. Int.* 19 65

[24] Thomas J K, Kurian J, Ittyachen M A and Koshy J 1995 *Mater. Lett.* 25 301

[25] Dusoulier L, Cloots R, Vertruyen B, Moreno R, Burgos-Montes O and Ferrari B 2011 *J. Eur. Ceram. Soc.* **31** 1075

[26] Closset R, Devendra Kumar N, Wera L, Dellicour A, Henrist C, Boschini F, Cloots R, Vanderbemden P and Vertruyen B 2013 *Mater. Lett.* **119** 154

[27] Fagnard J-F, Dirickx M, Ausloos M, Lousberg G, Vanderheyden B and Vanderbemden P 2009 *Supercond. Sci. Technol.* 22 105002

[28] Chiu R C, Garino T J and Cima M J 1993 *J. Am. Ceram. Soc.* **76** 2257

[29] Bauer C, Cima M, Dellert A and Roosen A 2009 *J. Am. Ceram. Soc.* 92 1178

[30] Besra L and Liu M 2007 *Prog. Mater. Sci.* 52 1

[31] Sarkar P, De D and Rho H 2004 *J. Mater. Sci.* **39** 819

[32] Lide D R (ed) *CRC Handbook of Chemistry and Physics* 85th edn (Boca Raton, FL: CRC Press) pp 6-150 and pp 6-151

[33] Barsoum M W 2003 *Fundamentals of Ceramics* (London: Taylor and Francis) pp 302-15 and pp 334-337

[34] Lide D R (ed) *CRC Handbook of Chemistry and Physics* 85th edn (Boca Raton, FL: CRC Press) pp 12-220

[35] Zeisberger M, Latka I, Ecke W, Habisreuther T, Litzkendorf D and Gawalek W 2005 *Supercond. Sci. Technol.* 18 S202

[36] Aravind M and Fung P C W 1999 *Meas. Sci. Technol.* **10** 979

[37] Wu B, Du Y, Tang H, Du P, Qin X and Zhang L 1995 *J. Phys. Chem. Solids* 57 1211

[38] MacManus-Driscoll J L, Bravman J C and Beyers R B 1995 *Physica* C **241** 401

[39] Costa G A and Mele P 2002 *Physica* C **372-376** 1174

[40] Murakami M 1992 *Melt Processed High Temperature Superconductors* (Singapore: World Scientific) pp 47-54

[41] Hari Babu N, Jackson K P, Dennis A R, Shi Y H, Mancini C, Durrell J and Cardwell D A 2012 *Supercond. Sci. Technol.* 25 075012

[42] Vanderbemden P, Ausloos M and Cloots R 2000 *Mater. Res. Soc. Symp. Proc.* **659** 118.4

[43] Devendra Kumar N, Rajasekharan T and Seshubai V 2011 *Supercond. Sci. Technol.* 24 085005

[44] Iida K, Hari Babu N and Cardwell D A 2007 *Supercond. Sci. Technol.* 20 1065

[45] Bean C P 1962 *Phys. Rev. Lett.* 8 25038

[46] Kim Y B, Hempstead C F and Strand A R 1962 *Phys. Rev. Lett.* 9 306

[47] Fagnard J-F, Denis S, Lousberg G, Dirickx M, Ausloos M, Vanderheyden B and Vanderbemden P 2009 *IEEE Trans. Appl. Supercond.* 19 2905

[48] Niculescu H, Schmidmeier R, Topolski B and Gielisse P J 1994 *Physica* C **229** 105

[49] Muller R, Fuchs G, Grahl A and Kohler A 1993 *Supercond. Sci. Technol.* 6 225

[50] Itoh M, Ohyama T, Minemoto T, Numata K and Hoshino K 1992 *J. Phys. D: Appl. Phys.* 25 1630

[51] Ganesan V, Srinivasan R, Aswathy S, Chandrasekharan K D, Subba Rao G V and Rajasekharan T 1993 *Solid State Commun.* 87 1081

[52] Willis J O, McHenry M E, Maley M P and Sheinberg H 1989 *IEEE Trans. Magn.* 25 2502

[53] Karthikeyan J, Paithankar A S, Chaddah P and Sreekumar K P 1991 *Supercond. Sci. Technol.* 4 250

[54] Pavese F, Bianco M, Andreone D, Cresta R and Rellecati P 1992 *Physica* C **204** 1

[55] Grenci G, Denis S, Dusoulier L, Pavese F and Penazzi N 2006 *Supercond. Sci. Technol.* 19 249